Energy Conversion and Management: X 23 (2024) 100667

Contents lists available at ScienceDirect

Energy Conversion and Management: X

journal homepage: www.sciencedirect.com/journal/energy-conversion-and-management-x

A sustainable self-generating system driven by human energy for wearable safety solutions

Se Yeong Jeong [a,1], Wei-Chieh Liu [a,1], Jae Yong Cho [b,1], Yu Jin Oh [c], Anuruddh Kumar [a], Sang Bum Woo [a], Seong Do Hong [a], Chul Hee Ryu [a], Tae Hyun Sung [a,*]

[a] Department of Electrical Engineering, Hanyang University, Wangsimni-ro, Seongdong-gu, Seoul, Republic of Korea
[b] Life Solution Team, Samsung Research (Samsung Electronics), Seoul 06765, Republic of Korea
[c] Department of Clothing & Textiles, Hanyang University, Wangsimni-ro, Seongdong-gu, Seoul, Republic of Korea

ARTICLE INFO

Keywords:
Electromagnetic energy generator
Energy harvesting
Human energy
Wearable device
Safety

ABSTRACT

With the improvement in people's quality of life, the requirements for health and safety are also increasing. While many wearable devices are available, those wearable devices specifically designed for the safety of night workers have yet to be effectively utilized. A survey conducted with 100 night workers revealed that they have expressed concerns about their safety and that of their colleagues due to lack of visibility while working on the road at night. To address this issue, a wearable electromagnetic energy generator was designed as a permanent solution to increase the visibility of night workers by illuminating LEDs and reduce the discomfort associated with wearable devices. The generator can be integrated with uniforms and converts the kinetic energy generated by the human body during work into electrical power. The generator achieved a maximum output power of 4.28 mW under 2.8 Hz, with a power density is 51.56 $\mu W/cm^3$. The LED brightness driven by the generator reached 218 Lux. To ensure user customization, the Living Lab strategy was employed, allowing direct user participation during the development process and incorporating improvements based on their feedback. After gathering feedback from the workers, the uniform was redesigned and revised multiple times. Ultimately, the product received high satisfaction scores and was successfully delivered to local municipalities. This paper details a comprehensive study covering the process from needs survey to product design.

1. Introduction

Recently, numerous studies have shown significant progress in the field of energy harvesting, particularly for wearable and self-powered electronic devices [1–4]. The primary purpose of energy harvesting devices is to collect and convert wasted energy into renewable electrical energy [5–7]. These devices can extend battery life and potentially enable self-sustaining systems.

There have been numerous studies on energy harvesting technologies, encompassing piezoelectric [8,9], electromagnetic [10–12], triboelectric [13–15], wind [16,17], and solar [18,19] methods. Research efforts have focused on enhancing the efficiency and miniaturization of these devices to render them more practical and suitable for everyday use. Among these diverse methods, energy generated through human movement is particularly advantageous when applied to wearable devices [20,21].

The development of energy self-sufficient systems through energy harvesting technology has the potential to reduce or eliminate the need for external power sources, offering greater flexibility, autonomy, and reliability in remote or resource-limited environments. Among these energy harvesting technologies, electromagnetic energy generators dominate in harvesting energy from the human body due to their high power output and high durability [22–25].

Traditional methods for research and development (R&D) are often unidirectional, primarily from the researchers to the users. Researchers typically develop products based on their own expertise inside a laboratory, focusing solely on technological advancement without user feedback. This approach results in low user satisfaction due to the lack of communication between researchers and end-users. To bridge this gap, we employed the Living Lab research strategy [26,27]. Living Lab approach allows users to directly participate in the research and development process, facilitating the creation of customized products

* Corresponding author.
E-mail address: sungth@hanyang.ac.kr (T.H. Sung).
[1] Contributed equally to this work.

https://doi.org/10.1016/j.ecmx.2024.100667
Received 18 April 2024; Received in revised form 21 June 2024; Accepted 14 July 2024
Available online 19 July 2024

that meet their needs. The strategy emphasizes starting innovation with users' ideas, experiences, knowledge, and daily requirements through bidirectional communication. The Living Lab consists of five main steps: Empathize, Define, Ideate, Prototype, and Test, as shown in Fig. 1. The process was rigorously followed in the development of a human motion-based electromagnetic energy generator (HMEG), incorporating continuous feedback from night workers.

A preliminary survey conducted among 100 night workers revealed that 91.3 % had felt threatened or had encountered accidents while working. Specifically, 55.8 % reported either experiencing accidents themselves or knowing coworkers who had experienced accidents, and 35.6 % felt threatened despite not having had any accidents. Traffic accidents were the most frequently reported incidents, accounting for 64.7 % of the responses, as shown in Fig. 2. These statistics underscore the critical need for enhanced safety uniforms that improve the visibility of night workers to drivers.

Street cleaners, who often work in low-visibility conditions, face similar risks. Despite wearing uniforms with reflective tape, the effectiveness of this tape diminishes over time due to frequent washing and its reliance on external light sources, making it ineffective in dark areas. To improve visibility, LED vests have been introduced. However, these vests present challenges such as the need for periodic battery recharging or replacement, added bulk, and the inability to wash them. Consequently, the adoption of LED vests among street cleaners has been limited. The battery issue in LED vests can be solved with an energy-generating devices, which convert wasted energy into renewable electrical energy.

Many researchers have developed various electromagnetic energy generators using human movement. [25,28–31]. Although many studies are in progress, there are few successful cases of practical application. For this reason, this work proposes an LED- integrated safety uniform powered by a human motion-based electromagnetic energy generator (HMEG), as shown in Fig. 3. This generator replaces traditional batteries, generating power through the user's movements. The integrated uniform eliminates the need for additional vests, addressing both battery and bulk issues. This innovation not only maintains visibility but also enhances the safety and convenience of night workers, effectively reducing the risk of accidents.

2. Design and modeling of the HMEG

2.1. Design

Fig. 4 illustrates the schematic diagram of the proposed HMEG. The device comprises a bobbin and a housing unit, both produced using a 3D printer. The primary components include a main magnet (20 mm in diameter and 10 mm in height), an auxiliary magnet (5 mm in diameter and 1 mm in height), and a copper induction coil wound with 11,600 turns of 60 μm copper wire around the bobbin. The fixed disk magnet at the bottom of the housing facilitates electricity generation through the up-and-down movement of the central magnet. This movement is driven by the repelling forces between the magnets, creating a magnetic spring effect that suspends the central movable magnet. To maintain a compact design, the driving circuit is mounted above the bobbin, and a push switch is included to control the operation of the LEDs. The specifications and dimensions of the components are detailed in Table 1.

2.2. Simulation

To estimate the power of the HMEG, a simulation was conducted using COMSOL software, employing its electromagnetic module to encompass electrical, mechanical, and magnetic domains. The HMEG is shaped as a hollow cylinder, 40 mm in length, as depicted in Fig. 5(a). A copper coil is wound along the circumference of the cylinder. In practical applications, external disturbances cause the entire body of the HMEG to vibrate, resulting in the relative movement of the magnet along the cylinder's length. Fig. 5(b) illustrates the single degree of freedom (SDOF) model of the electromagnetic energy generator, using a linear spring-mass system, which can be expressed as the following equations:

$$\frac{m}{\theta}\ddot{z}(t)+\frac{c}{\theta}\dot{z}(t)+\frac{f_m(z(t))}{\theta}+i(t)=\frac{\ddot{m}}{\theta}\ddot{y}(t) \tag{1}$$

$$\varepsilon(t)=\dot{x}(t)\theta \tag{2}$$

where x(t) and y(t) are the displacement of main magnet and housing, respectively, as shown in Fig. 5(a). z(t) represents the relative displacement between the magnet and coil; $\dot{z}(t)$ and $\ddot{z}(t)$ are the first and second derivative of z(t) with reference to time. $\varepsilon(t)$ denotes the electromagnetic force induced in the coil; c represents the viscous damping forces; f_m denotes the magnetic force between the main and auxiliary

Fig. 1. The development and application process of the HMEG based on the Living Lab.

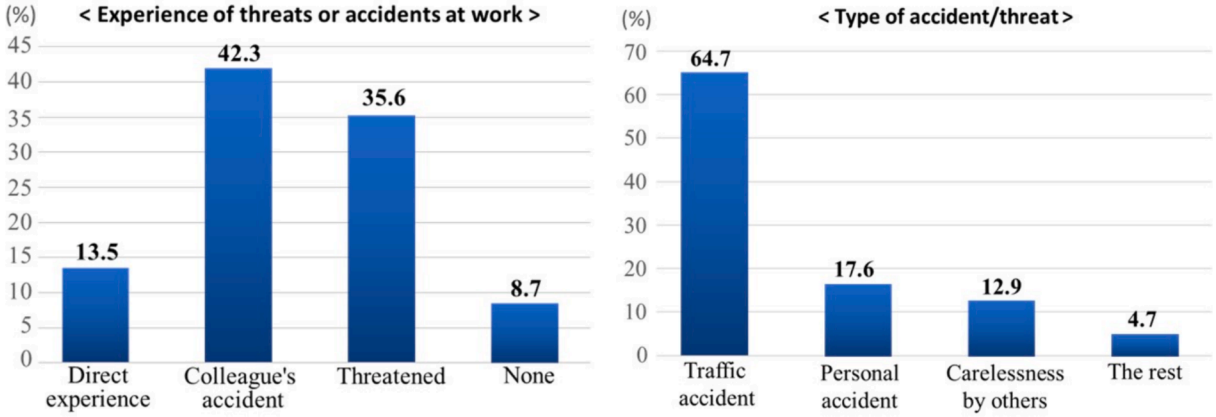

Fig. 2. Survey results on the experiences of night workers regarding threats and accidents.

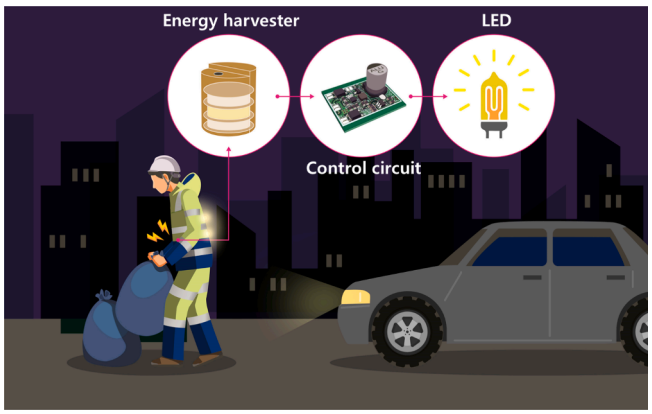

Fig. 3. The Conceptual design of the LED-integrated safety uniform with the HMEG in the work environment.

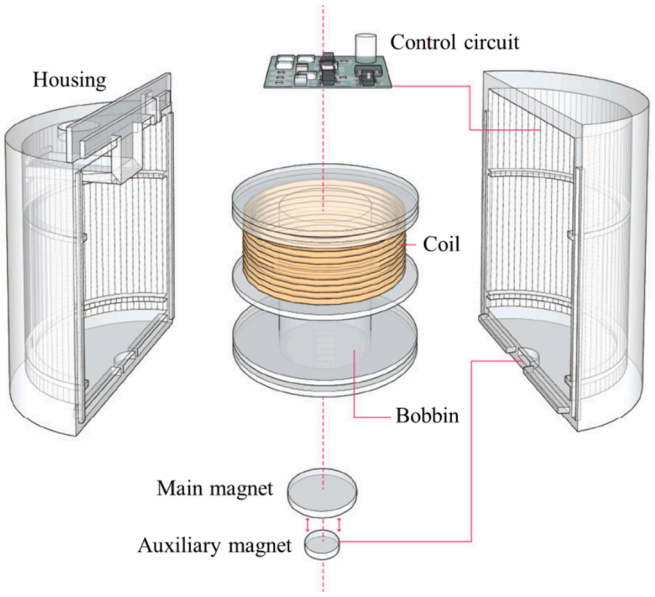

Fig. 4. The design of the HMEG.

magnet, and θ is the electromechanical coupling coefficient of the coil.

To validate the simulation model, the force between the main and auxiliary magnets was examined and compared with that reported in the literature. For this purpose, the magnetic field module of COMSOL was used without current, employing the same parameters as in the literature [32]. The output of this simulation is presented in Fig. 5(c), demonstrating excellent agreement with the literature results. Fig. 5(d) depicts the contour plot of the magnetic lines around these magnets at a specific distance.

Table 1
Specification of the HMEG.

Parameter	Value	Unit
Housing diameter	46	mm
Housing height	53	mm
Bobbin outer diameter	40	mm
Bobbin inner diameter	22	mm
Bobbin height	32	mm
Main magnet diameter	20	mm
Main magnet height	5	mm
Auxiliary magnet diameter	1	mm
Auxiliary magnet height	10	mm
Coil diameter	60	μm
Coil turns	11,600	–
Total volume	83.05	cm^3
Total mass weight	96	g

In the following simulation, the displacement of the main magnet was calculated in response to external disturbances affecting the HMEG. The HMEG was excited with a sinusoidal motion having an amplitude of 10 mm and a frequency of 2.8 Hz (human frequency). The main magnet moves identically to the body because the HMEG is rigidly attached to it. This causes the magnetic force to change between these two magnets. The main magnet moves along the length of the HMEG due to the repulsive force between the magnets, as shown in Fig. 6(a).

Furthermore, the voltage of the HMEG was investigated due to the movement of the main magnet surrounded by a copper coil. For this purpose, the electromagnetic fields of the AC/DC module from the COMSOL library were used for the HMEG. The relative displacement from the second simulation study was used as the input for the main magnet displacement in the simulation model. Due to this magnet movement, the flux changes inside the copper coil, generating the electromotive force (emf) in the coil according to Faraday's law. Fig. 6 (b) shows how the magnetic lines change inside the coil as the magnet moves. Fig. 6(c) shows the voltage resulting from the change in the magnetic flux inside the coil.

3. Results and discussion

3.1. Electrical output performance test

Experimental verification was performed to assess the reliability of the simulation results presented earlier. The experiment was conducted

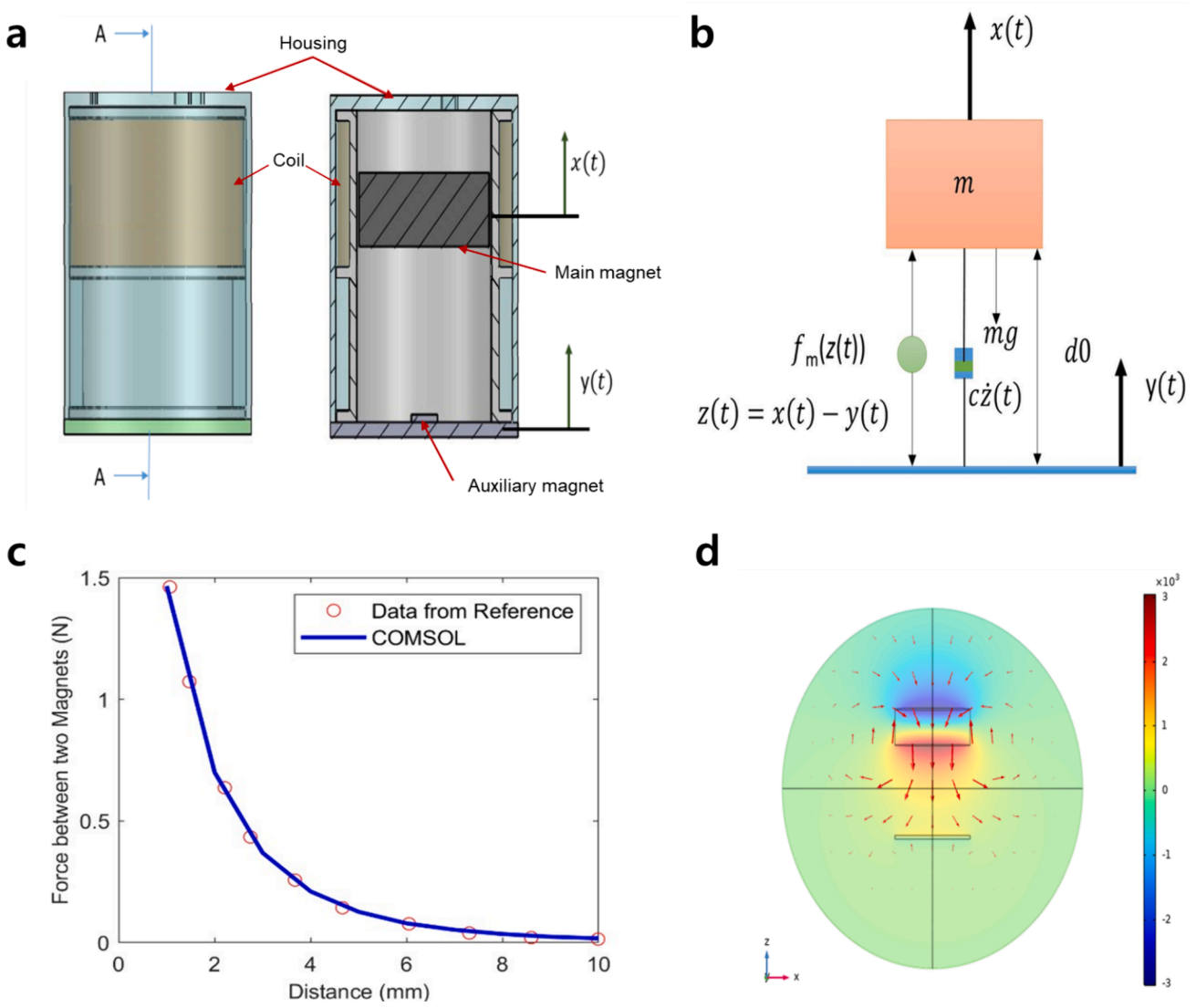

Fig. 5. (a) Schematic of the HMEG. (b) Free body diagram of the magnet and generator body under base vibration conditions. (c) The magnetic force between the main and auxiliary magnets. (d) Contour plot of the magnetic line distribution.

by attaching the HMEG vertically to a pushing tester at 2.8 Hz, which falls within the frequency range generated by a human, as shown in Fig. 7(a). The DPO4054B oscilloscope was used to measure the output voltage. Fig. 7(b) shows the open-circuit voltage of the HMEG at a vertical displacement of 10 mm in detail. Fig. 7(c) displays the voltage results for the 6 to 14 mm range. The voltage of the HMEG ranges from 13 V (at 6 mm) to 21 V (at 14 mm). The voltage generated by the HMEG increases as the vertical displacement increases. Subsequently, the electrical output performance test was conducted over a resistance range of 2 to 70 kΩ at 2.8 Hz, as shown in Fig. 7(d). The maximum power is 4.28 mW at a resistance of 10 kΩ. Fig. 7(e) shows that the maximum voltage increases dramatically from 6 to 14 mm.

3.2. Comparison with devices in literature

To compare the test results with other low-frequency vibration electromagnetic energy harvesters used in human activities, power density ($\mu W/cm^3$) is used as the evaluation indicator. Table 2 presents the comparison results, confirming that the HMEG proposed in this study achieves higher power generation and energy density at low frequencies. This not only demonstrates its outstanding performance at low frequencies but also enhances its suitability for harvesting energy from human activities. The superior energy density makes the HMEG a promising candidate for powering wearable and portable devices.

3.3. Human application test

To directly apply the results to night workers, the experiment was conducted based on human movements and the positions of the HMEG as shown in Table 3. Case #1 involves placing the HMEG inside the arm pocket during sweeping, while Case #2 involves placing it inside the arm pocket while raising the hand. Case #3 entails placing the HMEG inside the arm pocket during walking, and Case #4 involves placing it inside the front pocket near the thigh while walking.

Fig. 8(a) shows the installation locations of the HMEG, specifically the arm pocket (i) and front pocket (ii). Fig. 8(b) displays the voltage waveform generated by the HMEG when placed in the arm pocket during a single sweeping motion, reaching a maximum voltage of 6 V. Fig. 8(c) shows the waveform of the HMEG inside the arm pocket during hand-raising, with a maximum voltage of 17 V. In these two cases, a temporary voltage was observed.

To induce a continuous voltage, a walking test was conducted with the HMEG positioned in both the arm pocket and front pocket. Fig. 8(d) reveals the maximum voltage of 12 V generated when the HMEG was in

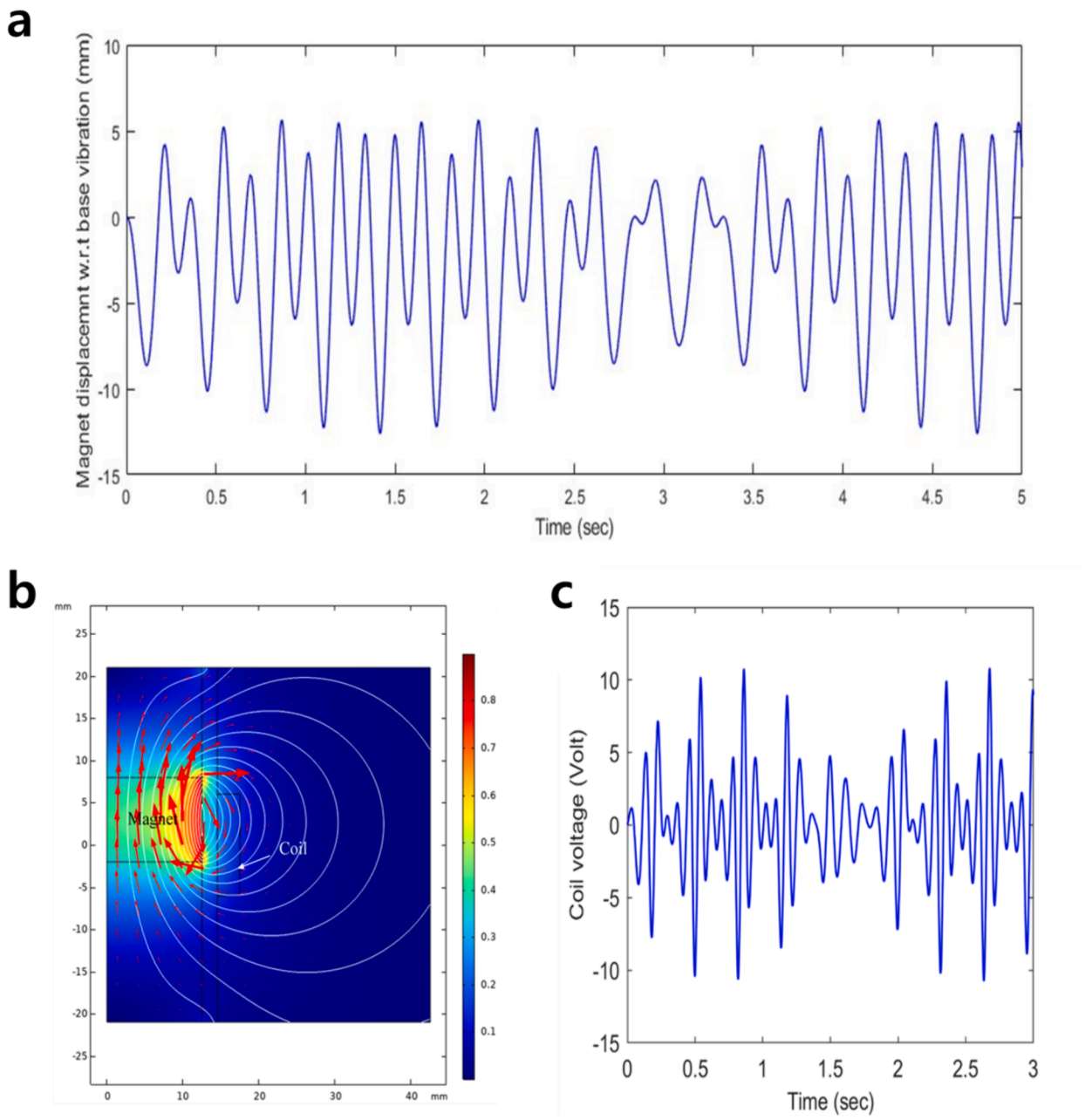

Fig. 6. (a) Displacement of the main magnet due to an external vibration. (b) Contour plot of the magnetic field line around the copper coil. (c) Voltage due to the change in the magnetic flux around the coil.

the arm pocket during walking test. Fig. 8(e) demonstrates an increased voltage of 21 V when the HMEG was moved to the front pocket near the thigh under the same walking condition. These findings indicate that positioning the HMEG in the front pocket near the thigh yields higher energy generation compared to the arm pocket during walking postures. Considering the voltage waveforms and the predominance of the walking movements during work, it was concluded that attaching the HMEG to the inside of the front pocket is the most effective location.

Fig. 9 shows the test results of the output voltage and energy charging during the continuous movement of a night worker over 45 s. To determine the optimal installation location for the HMEG, the test was conducted on the arm and in the front pocket near the thigh, involving sweeping, raising hand, and walking movements. To ensure the reliability of the findings, the test was repeatedly conducted with three different testers (#1∼ #3). Fig. 9(a) shows the voltage waveform of the HMEG inside the arm pocket during continuous floor sweeping, reaching a maximum voltage of 3 V. Fig. 9(b) shows the voltage waveform when the HMEG is positioned in the arm pocket during repeated hand-raising motion, producing a voltage of approximately 2.8 V. During the walking of a night worker, the output tests were conducted at two locations: the arm and front pockets, as shown in Fig. 9(c) and Fig. 9 (d). Output voltages of 4.5 and 6 V were recorded when the HMEG was located in the arm pocket and front pockets during walking respectively. A comparison of these results indicates that walking motion induces relatively high voltage.

Subsequently, an energy storage test was conducted for an actual LED application. Continuous sweeping resulted in an average charged voltage of approximately 2 V and the stored energy of approximately 2 mJ ($E=1/2C\bullet V^2$, where C=1000 μF), as shown in Fig. 9(e). In Fig. 9(f), results indicate that with the HMEG positioned inside the arm pocket during hand-raising, the average charged voltage and energy generated were 1.7 V and 1.4 mJ, respectively. Fig. 9(g) demonstrates a charged

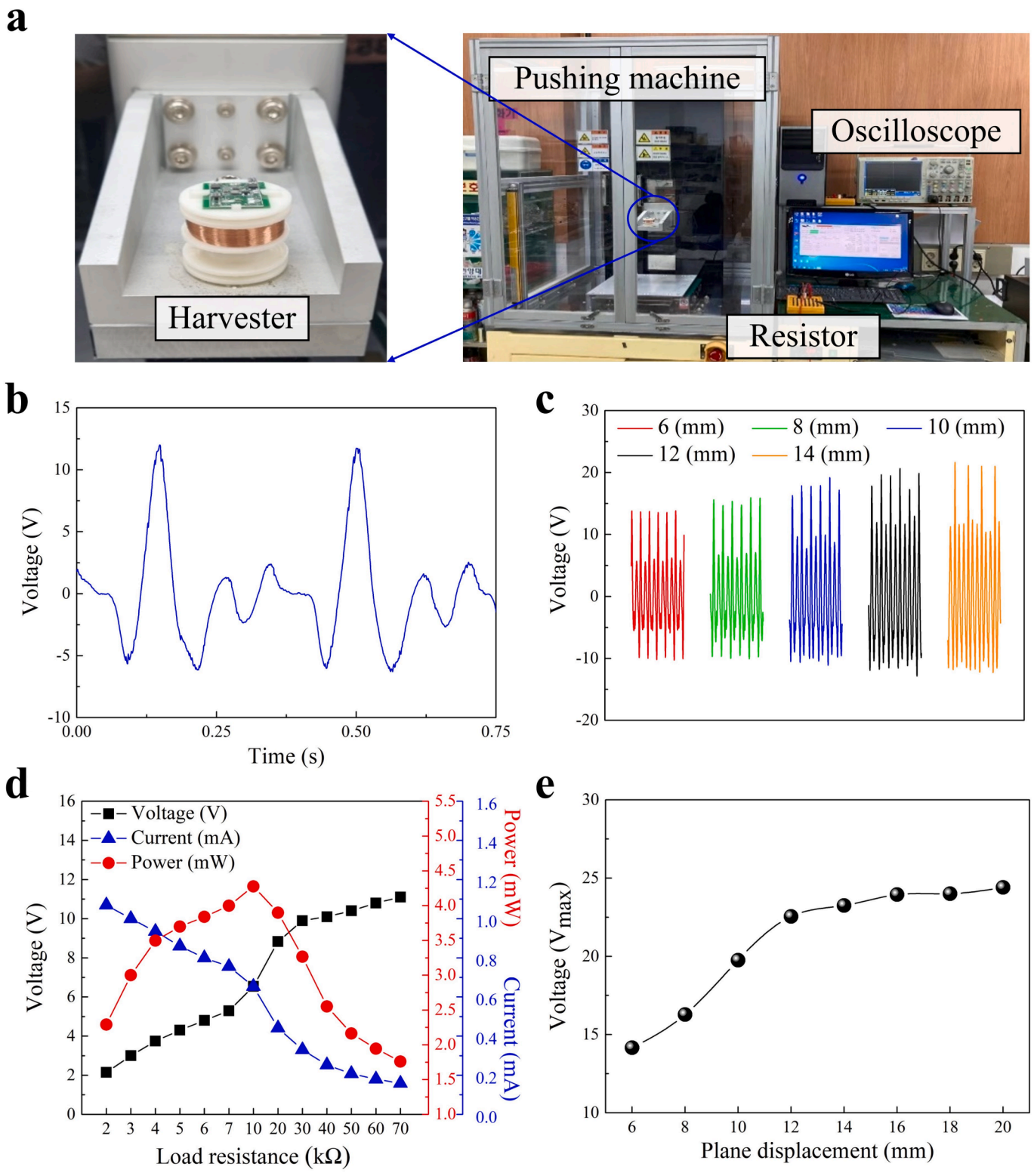

Fig. 7. (**a**) Experimental setup for measuring the power generation of the HMEG. (**b**) The open-circuit voltage of the HMEG at a vertical displacement of 10 mm. (**c**) The open-circuit voltage waveform generated by the HMEG at different vertical displacements. (**d**) The output performance test at different load resistances from 2 to 70 kΩ at 2.8 Hz. (**e**) Maximum voltage according to the vertical displacements.

voltage of 2.15 V (equivalent to 2.31 mJ) when the HMEG was situated inside the arm pocket during walking. Fig. 9(h) shows the charged voltage of 4 V and 8 mJ when the HMEG was relocated to the front pocket during walking. In summary, Fig. 9(i) presents the total charge results, highlighting the optimal output condition when the HMEG is placed in the front pocket during walking. Consequently, based on these findings, subsequent application tests employed the HMEG inside the front pocket during walking movements.

Table 2
HMEG in the literature and in this study.

Reference	F (Hz)	Power (mW)	Vol. (cm^3)	Power density ($\mu W/cm^3$)
[12]	3.45	1.4	50	28
[28]	10	0.33	78	4.23
[29]	–	0.86	30	28.67
[30]	–	0.38	10	38
[31]	1	0.0613	20	3.07
This work	2.8	4.28	83	51.56

Table 3
Experimental cases according to the human movement and locations of the HMEG.

Case	Movement	Location
#1	Sweeping	Arm pocket
#2	Raising hand	Arm pocket
#3	Walking	Arm pocket
#4	Walking	Front pocket

3.4. LED application test

Because the voltage generated by the HMEG fluctuates depending on the mechanical input condition, a converter that ensures a steady voltage supply is required as a power source for the LED, as shown in Fig. 10(a). The AC voltage generated by the HMEG is stored in the input capacitor (C_i) through the rectifier (D_{rect}) and is connected to the input terminal of the step-down converter (TPS62125) with the under voltage lock out (UVLO) [33]. The UVLO function is necessary to operate the LEDs for a certain period, even if the HMEG stops moving and does not generate power. The converter remains in shutdown mode until the voltage of the input capacitor (V_i) reaches the threshold voltage ($V_{IN\_startup}$). If the V_i exceeds the threshold voltage, the converter enters the operating mode, and (V_{out}) is connected to the square-wave generator and the LEDs. The energy stored in C_i is transferred to the load, and if the HMEG is continues to generate power, the voltage of C_i will be maintained. otherwise, the converter will return to the shutdown mode if V_i falls below V_{IN_stop}. The input voltage level $V_{IN\_startup}$, at which the device starts up, is set by the resistors R1 and R2.

$$V_{IN\_startup} = V_{EN\_TH\_ON} \times \left(1 + \frac{R_1}{R_2}\right) = 1.2V \times \left(1 + \frac{R_1}{R_2}\right) \quad (3)$$

The input voltage level V_{IN_stop}, at which the device will stop operating, is set by R_1, R_2 and R_3.

$$V_{IN\_stop} = V_{EN\_TH\_OFF} \times \left(1 + \frac{R_1}{R_2 + R_3}\right) = 1.15V \times \left(1 + \frac{R_1}{R_2 + R_3}\right) \quad (4)$$

It is not easy to continuously drive the LEDs with the amount of energy generated by human motion because a significant amount of power is required to keep the LEDs constantly on. Thus, the power consumption can be reduced by incorporating a flashing function, allowing the LED to turn on/off periodically. The voltage generated by the square-wave generator, consisting of a comparator (TLV3701), is used to turn a MOSFET on and off. When the voltage applied to the gate terminal of the MOSFET exceeds threshold voltage (V_{th}), the MOSFET turns on, allowing current to flow to the LED, which then illuminates. Conversely, when the gate voltage does not exceed V_{th}, the MOSFET turns off, and the LED is turned off. The output remains high while C1 charges and low while C1 discharges. Because the capacitor charges through R10 and R11 and discharges through R11, the duty cycle that drives the LED can be controlled by adjusting the ratio of these resistances [34]. When the capacitor voltage reaches 5.6 V, the LED will

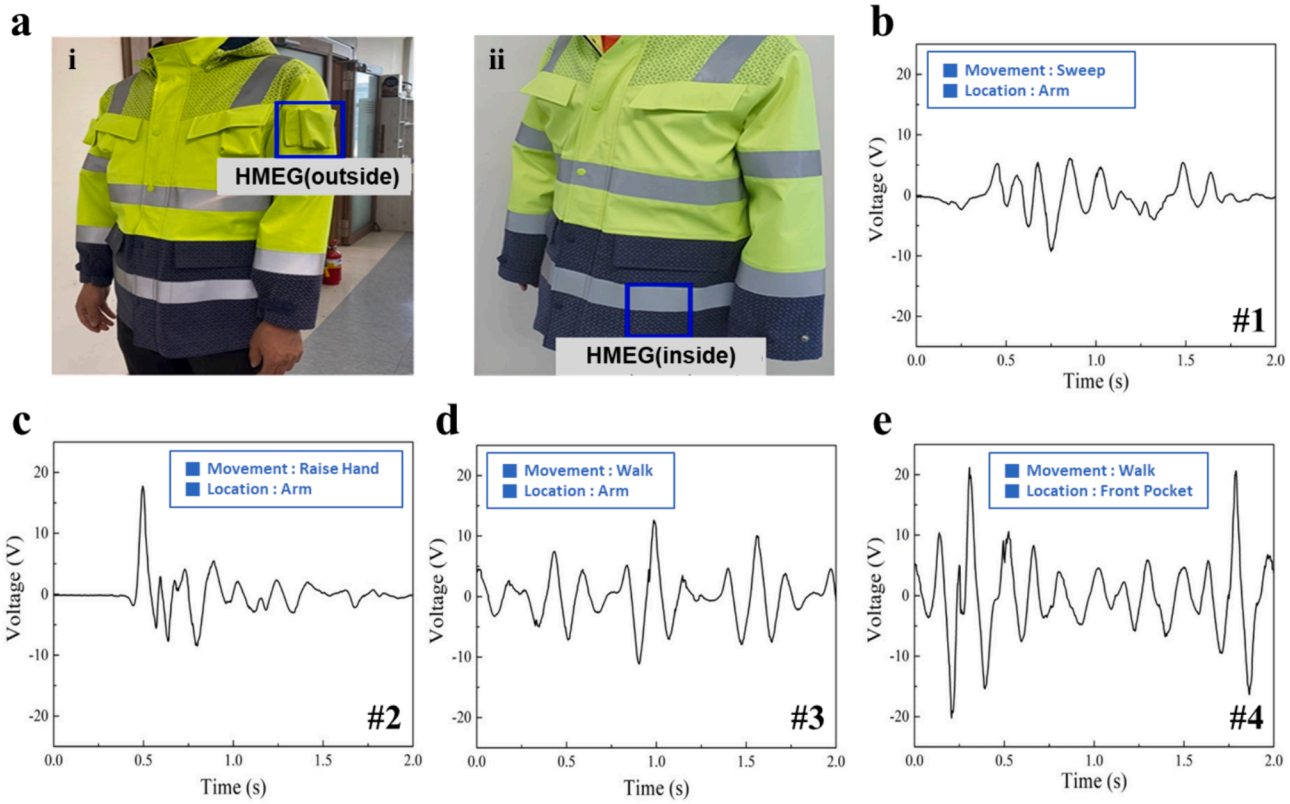

Fig. 8. (a) The positions (i-outside and ii-inside pocket) where the HMEG was attached. The voltage wave pattern generated by the HMEG attached to the arm position for (b) the sweeping movement, (c) the raising hand movement, and (d) the walking movement. (e) The voltage wave pattern generated by the HMEG attached to the front pocket position for the walking movement.

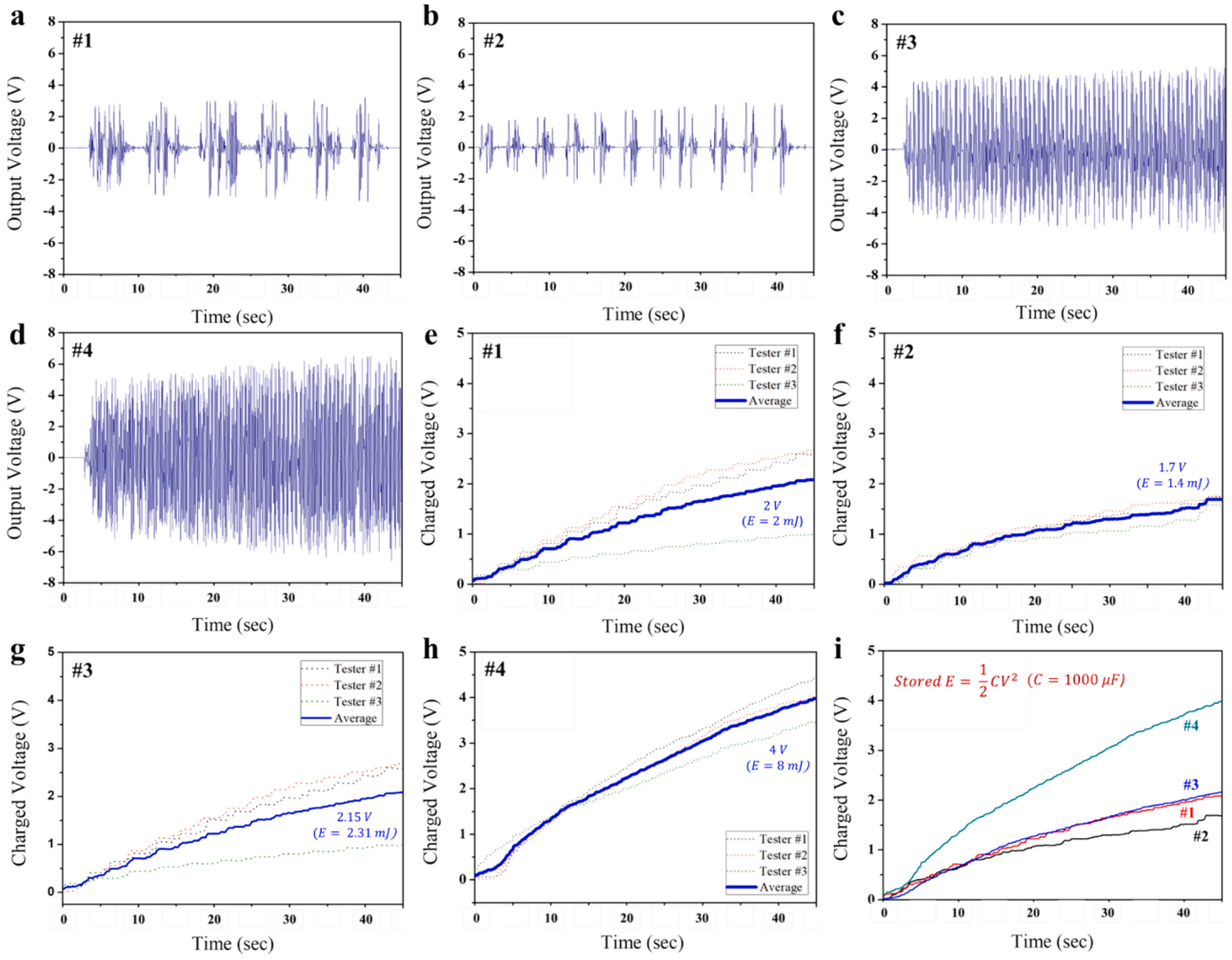

Fig. 9. The open-circuit voltage of the HMEG in (a) Case #1 (Movement: Sweeping; Location: Arm pocket), (b) Case #2 (Movement: Raising hand; Location: Arm pocket), (c) Case #3 (Movement: Walking; Location: Arm pocket) and (d) Case #4 (Movement: Walking; Location: Front pocket). The charged voltage of the HMEG in the 1000 μF capacitor of (e) Case #1, (f) Case #2, (g) Case #3 and (h) Case #4. (i) The total charged voltages of the HMEG in the 1000 μF capacitor.

operate for approximately 20 s even without movement, as shown in Fig. 10(b).

The PMC consists of a 2.2 × 2 cm^2 PCB integrated with a bobbin, as shown in Fig. 10(c). A manual switch positioned above the HMEG allows users to deactivate the circuit when the LED is not in use. In Fig. 10(d), four high-brightness chip LEDs, emitting light over a long distance are mounted on a single PCB, with each LED is connected in parallel. Initially, the PCB was manufactured in a flexible type for insertion into the uniform. However, due to repeated bending during uniform washing, the LEDs were prone to detachment, prompting a redesign into a rigid type. The LED PCB features positive and negative terminals, facilitating electrical connection to the PMC via a connector. This connector allows easy separation from the HMEG during uniform washing.

3.5. Design of LED-integrated safety uniform

To develop safe work uniforms, this study collaborated with a deep Living Lab team consisting of 56 night workers from Jung-gu and Nowon-gu in Seoul. After extensive discussions and surveys, the results indicated that the most desired feature of the uniforms was safety, followed by functionality and mobility. To enhance the safety of the uniforms, the positions of the reflective prints and LED lights were carefully designed to ensure clear visibility to drivers at night. However, increasing the area of *retro*-reflective material to enhance nighttime visibility reduces the area of fluorescent material, thus decreasing daytime visibility. To address this issue and enhance the *retro*-reflective effect, *retro*-reflective printing was introduced into the existing sanitation uniforms. The developed uniform design includes a substrate area of 1.235 m^2 and a *retro*-reflective material area of 0.301 m^2, meeting the requirements of KS K ISO 20471:2013 for visible material area for a Class 3 garment, which mandates a substrate area of at least 0.80 m^2 and a *retro*-reflective material area of at least 0.20 m^2. Initially, the LEDs were placed on the front and back of the safety uniform, as shown in Fig. 11(a), but uniform-wearing test revealed glare problems from the front-mounted LEDs. Consequently, the front-positioned LEDs were relocated to the back of the uniform, as shown in Fig. 11(b). In subsequent tests, feedback indicated that the LEDs positioned on the upper back were obscured by the cap and that having LEDs only on the back made it difficult for users to verify their functionality. Taking into account this feedback, the LEDs positioned on the upper back were lowered to prevent obstruction by the cap, and LED indicators were attached to the lower front of the uniform to ensure they do not dazzle the user's eyes., as shown in Fig. 11(c). Fig. 11(d) illustrates the placement of the internal HMEG, wires, and cables within the uniform. The new uniform design integrates LEDs and wiring in a way that allows for washing without altering the original wearability of the uniform. To enhance functionality, the uniform elements were designed based on user needs. Considering the outdoor working environment of sanitation workers, breathable and waterproof materials were used to protect against rain

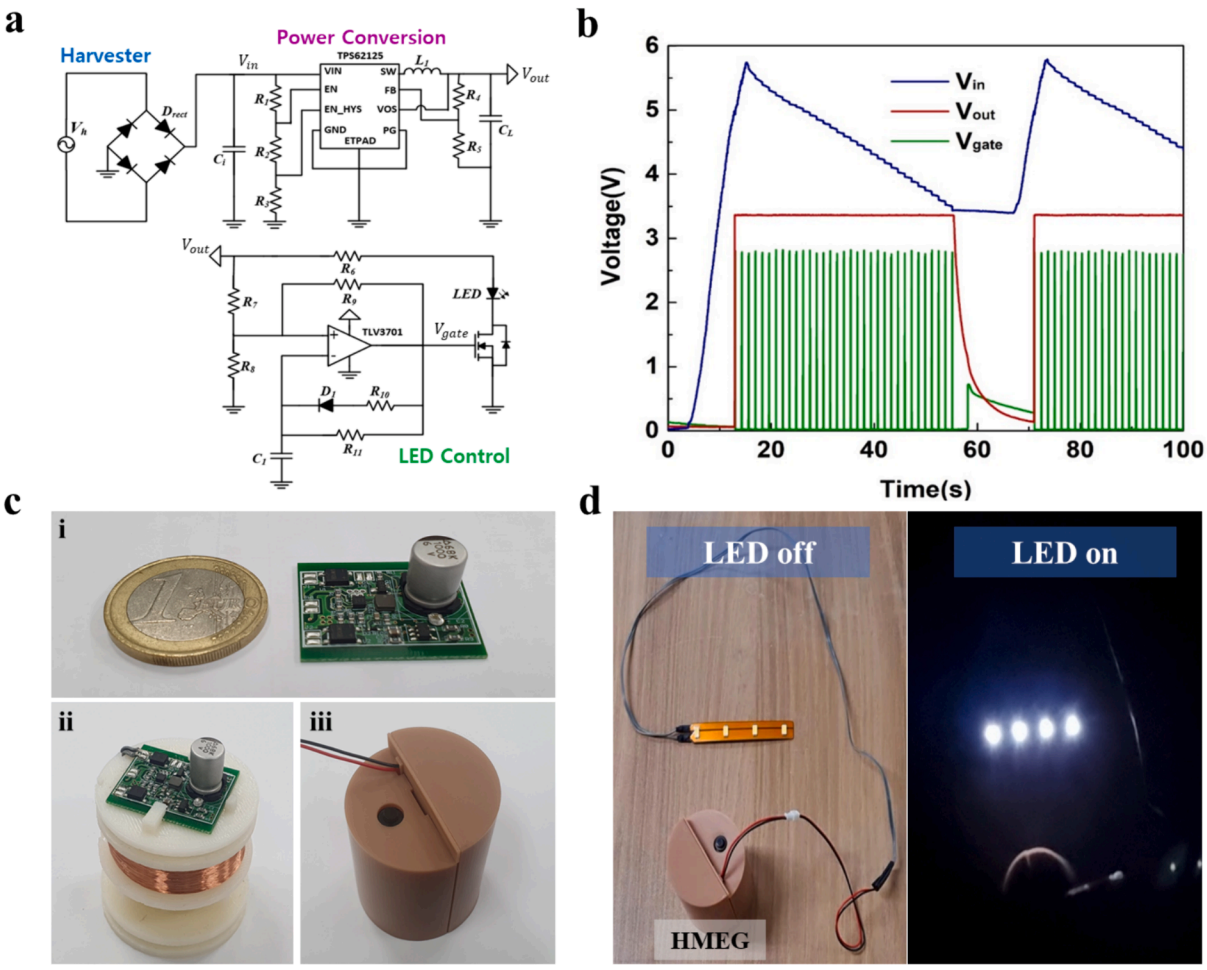

Fig. 10. (a) Driving circuit diagram of Power Management Circuit (PMC). (b) Input/output voltage and gate voltage of the driving circuit. (c) Actual photographs of (i) PMC with (ii) the HMEG and (iii) housing. (d) Light on/off test using the HMEG.

and wind. Dark-colored materials were used for the torso and cuffs, which are prone to staining, and ribbed knit fabrics and Velcro width adjusters were added to the cuffs and legs, which are prone to damage. The pockets were designed based on a survey of items commonly carried by sanitation workers, ensuring appropriate sizes, convenient opening and closing directions, and a secure locking mechanism.

To improve the mobility of the safety uniform, the HMEG was securely stored inside the uniform to ensure comfort during wear and movement, as shown in Fig. 11(e). Given that the HMEG generates power through vertical movement, it was securely fixed in an upright position using a trapezoidal rectangular column shape and rubber anti-slip strips. For easy installation and removal of the HMEG, a zipper was used at the top for opening and closing, and a wire hole for connecting the LEDs was created in the middle of the inner pocket using buttonhole stitching, as shown in Fig. 11(f). Fig. 11(g) and (h) depict the final LED-integrated safety uniform that was produced.

3.6. Performance evaluation for waterproof and dustproof

To ensure that the LED attached to the uniform operates normally even in extreme environments, the reliability of the LED-integrated safety uniform was evaluated through a waterproof and dustproof test (IPXX) conducted by a specialized testing institute. The test followed the KS C IEC 60523:2013 standard. A sample was placed in the test chamber and exposed to talc dust (2 kg/m^3) for 8 h, as shown in Fig. 12(a). After 8 h, the LEDs were turned on to confirm that they operated normally, as shown in Fig. 12(b). Then, the sample was submerged in a water tank at a depth of 1 m for 30 min, as shown in Fig. 12(c). After 30 min, the LEDs were turned on to confirm that they operated normally, as shown in Fig. 12(d). The LED-integrated safety uniform passed the IP57 waterproof and dustproof test, and the certification was obtained from the specialized testing institute. Additionally, a washing test was performed using a home washing machine, where the uniform was washed more than 30 times. The product's performance was successfully evaluated by verifying that the LED operated normally after repeated washing.

3.7. Satisfaction evaluation

To evaluate the satisfaction with the LED-integrated safety uniform, 94 sanitation workers wore the uniform during their work shifts, as shown in Fig. 13. Field interviews were conducted during their working hours, and additional feedback was obtained through a questionnaire. The questionnaire consisted of items related to "Uniform Design and Comfort" and "LED and Self-Power Generation Device.".

97 % of the respondents expressed an overall positive reaction to the new uniform design. Particularly, they were satisfied with the dark-colored areas on parts of the uniform that are prone to getting dirty. They also perceived the overall design as very sophisticated.

96 % of the respondents indicated that the LED illumination did not cause any discomfort to their eyes. This suggests that the placement of the LEDs was appropriately selected. Additionally, 96 % of the respondents felt that the LED integration significantly enhanced their safety, demonstrating a high level of effectiveness. Furthermore, 89 % of the respondents were satisfied with the placement of the HMEG,

Fig. 11. Front and back of the LED-integrated safety uniform: (a) first, (b) second, (C) third uniform. (d) location of LEDs and HMEG. (e) HMEH in the inner pocket (f) pocket structure. actual product pictures: (g) front-side view, (h) back-side view of the LED-integrated safety uniform.

reporting that the HEMG did not impede their work.

The uniform-related items received an average score of 92.1, while the LED and the HMEG items received an average score of 90.7. The overall satisfaction score for the LED-integrated safety uniform was 91.4. In general, the sanitation workers were highly satisfied with the uniform, validating its potential for practical application and distribution to local government for real-world use.

4. Conclusion

This work successfully designed and manufactured a human-based electromagnetic energy generator (HMEG) for night workers. The HMEG operates efficiently at low frequencies to power LED lights, ensuring the safety of workers at night. Utilizing a non-contact structure with repulsive forces between two magnets, the system provides high durability and low noise. With an overall volume of 83.05 cm3 and a

Fig. 12. (**a**) Dustproof test in chamber (IP5X), (**b**) LED operation check after dustproof test in water tank, (**c**) waterproof test (IPX7), (**d**) LED operation check after waterproof test.

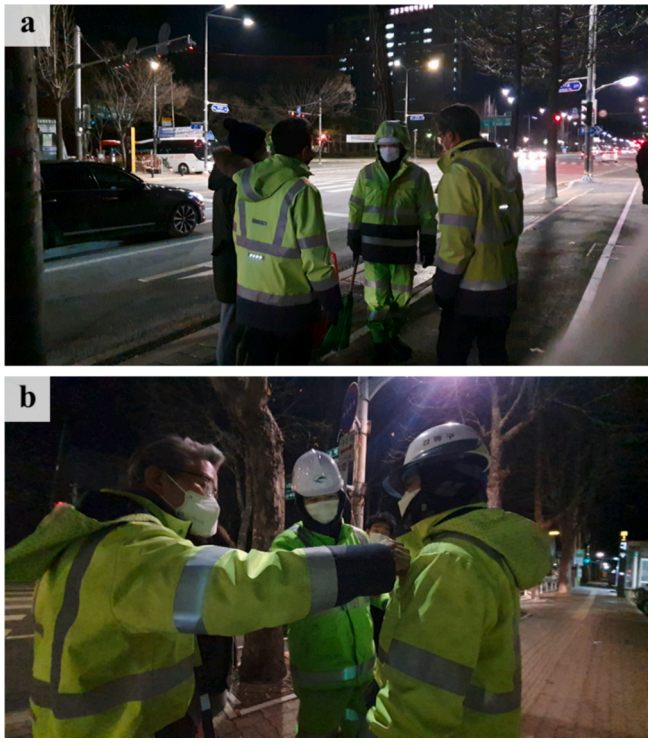

Fig. 13. Field interviews conducted during sanitation workers' shifts.

weight of only 96 g, the device minimizes the user's burden. The HMEG achieves a maximum output power of 4.28 mW at a load resistance of 10 kΩ, with a power density of 51.56 μW/cm^3, enabling it to efficiently drive LEDs. A specially designed circuit for controlling the LEDs helps conserve energy and extend their operational time. The HMEG-based safety system was developed for night worker, and improvements were made based on their feedback using the Living Lab process. Ultimately, repeated feedback demonstrated that safety clothing equipped with HMEG effectively improves the safety of night workers. The system was successfully used by night workers, achieving high satisfaction. With further optimization, HMEG has the potential to be applied to other wearable devices.

CRediT authorship contribution statement

Se Yeong Jeong: Writing – original draft. **Wei-Chieh Liu:** Writing – original draft. **Jae Yong Cho:** Writing – original draft. **Yu Jin Oh:** Conceptualization. **Anuruddh Kumar:** Methodology. **Sang Bum Woo:** Methodology. **Seong Do Hong:** Methodology. **Chul Hee Ryu:** Methodology. **Tae Hyun Sung:** Writing – review & editing, Supervision.

Declaration of competing interest

The authors declare that they have no known competing financial interests or personal relationships that could have appeared to influence the work reported in this paper.

Data availability

Data will be made available on request.

Acknowledgements

This research was supported by a program for fostering next-generation researchers in engineering by the National Research Foundation of Korea (NRF) funded by the Ministry of Science & ICT (No.

2017H1D8A2032495) and this work was also supported by "Human Resources Program in Energy Technology" of the Korea Institute of Energy Technology Evaluation and Planning (KETEP), granted financial resource from the Ministry of Trade, Industry & Energy, Republic of Korea. (No. 20204010600090).

Appendix A. Supplementary data

Supplementary data to this article can be found online at https://doi.org/10.1016/j.ecmx.2024.100667.

References

[1] Ganapathy SR, Salleh H, Azhar MKA. Design and optimisation of magnetically-tunable hybrid piezoelectric-triboelectric energy harvester. Sci Rep 2021:1–13. https://doi.org/10.1038/s41598-021-83776-y.
[2] Kim P, Nguyen MS, Kwon O, Kim Y-J, Yoon Y-J. Phase-dependent dynamic potential of magnetically coupled two-degree-of-freedom bistable energy harvester. Sci Rep 2016:1–10. https://doi.org/10.1038/srep34411.
[3] Van Toan N, Tuoi TTK, Van Hieu N, Ono T. Thermoelectric generator with a high integration density for portable and wearable self-powered electronic devices. Energ Conver Manage 2021:114571. https://doi.org/10.1016/j.enconman.2021.114571.
[4] Sun Q, et al. Smart band-aid: Multifunctional and wearable electronic device for self-powered motion monitoring and human-machine interaction. Nano Energy 2022:106840. https://doi.org/10.1016/j.nanoen.2021.106840.
[5] Gijón-Rivera C, Olazagoitia JL, Reyes-Avendaño JA. Design and development of a novel Four-Links rotational hybrid Energy-Harvesting suspension system compatible with conventional suspension technologies. Energ Conver Manage 2024;X:100572. https://doi.org/10.1016/j.ecmx.2024.100572.
[6] Yang Y-G, Cen M-H. Stochastic dynamics of an electromagnetic energy harvesting suspension with time-delayed feedback and fractional damping. Int J Non Linear Mech 2024;104766. https://doi.org/10.1016/j.ijnonlinmec.2024.104766.
[7] Luo A, Zhang Y, Xu W, Lu Y, and Wang F. Electromagnetic Energy Harvester with Inertial Rotary Structure for Human Motion Application at Ultra-Low Frequency. 2020 IEEE 33rd International Conference on Micro Electro Mechanical Systems (MEMS) 2020; 536-539. doi: 10.1109/MEMS46641.2020.9056319.
[8] Qiu C, et al. Transparent ferroelectric crystals with ultrahigh piezoelectricity. Nature 2020:350–4. https://doi.org/10.1038/s41586-019-1891-y.
[9] Li F, et al. Ultrahigh piezoelectricity in ferroelectric ceramics by design. Nat Mater 2018:349–54. https://doi.org/10.1038/s41563-018-0034-4.
[10] Asadi M, Ahmadi R, Abazari AM. Halbach Magnet Arrays in Electromagnetic Kinetic Energy Harvesters: A Review. Energy Conversion and Management: X 2024:100544. https://doi.org/10.1016/j.ecmx.2024.100544.
[11] Maharjan P, Bhatta T, Rasel MS, Salauddin M, Rahman MT, Park JY. High-performance cycloid inspired wearable electromagnetic energy harvester for scavenging human motion energy. Appl Energy 2019:113987. https://doi.org/10.1016/j.apenergy.2019.113987.
[12] Smilek J, Hadas Z, Vetiska J, Beeby S. Rolling mass energy harvester for very low frequency of input vibrations. Mech Syst Sig Process 2019:215–28. https://doi.org/10.1016/j.ymssp.2018.05.062.
[13] Sun B, Guo X, Zhang Y, Wang ZL, Shao J. A generalized model for a triboelectric nanogenerator energy harvesting system. Nano Energy 2024:109637. https://doi.org/10.1016/j.nanoen.2024.109637.
[14] Zou Y, Raveendran V, Chen J. Wearable triboelectric nanogenerators for biomechanical energy harvesting. Nano Energy 2020:105303. https://doi.org/10.1016/j.nanoen.2020.105303.
[15] Chen C, et al. Direct current fabric triboelectric nanogenerator for biomotion energy harvesting. ACS Nano 2020:4585–94. https://doi.org/10.1021/acsnano.0c00138.
[16] Calautit K, Johnstone C. State-of-the-art review of micro to small-scale wind energy harvesting technologies for building integration. Energy Convers Manage: X 2023:100457. https://doi.org/10.1016/j.ecmx.2023.100457.
[17] Akhter MZ, Ali AR, Jawahar HK, Omar FK, Elnajjar E. Enhanced energy extraction in small-scale wind turbines through slot-based passive blowing. Energ Conver Manage 2023;X:100400. https://doi.org/10.1016/j.ecmx.2023.100400.
[18] Chang S-Y, Cheng P, Li G, Yang Y. Transparent polymer photovoltaics for solar energy harvesting and beyond. Joule 2018:1039–54. https://doi.org/10.1016/j.joule.2018.04.005.
[19] Lau D, et al. Hybrid solar energy harvesting and storage devices: The promises and challenges. Mater Today Energy 2019:22–44. https://doi.org/10.1016/j.mtener.2019.04.003.
[20] Li J, Dong Y, Park JH, Yoo J. Body-coupled power transmission and energy harvesting. Nat Electron 2021:1–9. https://doi.org/10.1038/s41928-021-00592-y.
[21] Zhang Y-H, Lee A, Lee C-H. Design and Application of Piezoelectric and Electromagnetic energy Harvesters for Mechanical Energy Harvesting in the Human-body: A Review. Sens Actuators, A 2024:115207. https://doi.org/10.1016/j.sna.2024.115207.
[22] Masood Ahmad M, Ullah KF. Two degree of freedom vibration based electromagnetic energy harvester for bridge health monitoring system. J Intell Mater Syst Struct 2021:516–36. https://doi.org/10.1177/1045389X20959459.
[23] Ordonez V, Arcos R, Romeu J. A high-performance electromagnetic vibration energy harvester based on ring magnets with Halbach configuration. Energy Convers Manage: X 2022:100280. https://doi.org/10.1016/j.ecmx.2022.100280.
[24] Monaco ML, Russo C, Somà A. Numerical and experimental performance study of two-degrees-of-freedom electromagnetic energy harvesters. Energy Convers Manage: X 2023:100348. https://doi.org/10.1016/j.ecmx.2023.100348.
[25] Fan K, Zhang Y, Liu H, Cai M, Tan Q. A nonlinear two-degree-of-freedom electromagnetic energy harvester for ultra-low frequency vibrations and human body motions. Renew Energy 2019:292–302. https://doi.org/10.1016/j.renene.2019.01.105.
[26] Leal Filho W, et al. Living labs in the context of the UN sustainable development goals: state of the art. Sustain Sci 2023:1163–79. https://doi.org/10.1007/s11625-022-01240-w.
[27] Molinari M, Vogel JA, Rolando D, Lundqvist P. Using living labs to tackle innovation bottlenecks: the KTH Live-In Lab case study. Appl Energy 2023:120877. https://doi.org/10.1016/j.apenergy.2023.120877.
[28] Zhao L-C, et al. Magnetically modulated orbit for human motion energy harvesting. Appl Phys Lett 2019. https://doi.org/10.1063/1.5131193.
[29] Pan X, Zhang G, Yu N, Cai C, Ma H, Yan B. Low-frequency human motion energy scavenging with wearable tumbler-inspired electromagnetic energy harvesters. Int J Mech Sci 2024:109029. https://doi.org/10.1016/j.ijmecsci.2024.109029.
[30] Zhou N, Hou Z, Zhang Y, Cao J, Bowen CR. Enhanced swing electromagnetic energy harvesting from human motion. Energy 2021:120591. https://doi.org/10.1016/j.energy.2021.120591.
[31] Halim M, Rantz R, Zhang Q, Gu L, Yang K, Roundy S. An electromagnetic rotational energy harvester using sprung eccentric rotor, driven by pseudo-walking motion. Appl Energy 2018:66–74. https://doi.org/10.1016/j.apenergy.2018.02.093.
[32] Al-Ashtari W, Hunstig M, Hemsel T, Sextro W. Frequency tuning of piezoelectric energy harvesters by magnetic force. Smart Mater Struct 2012:035019. https://doi.org/10.1088/0964-1726/21/3/035019.
[33] Cho M-H, Lee W-H, Kim J-S, Sa Y-H, Kim H-S, Cha H-W. Development of undervoltage lockout (UVLO) circuit configurated Schmitt trigger. International SoC Design Conference (ISOCC) 2015;2015:59–60. https://doi.org/10.1109/ISOCC.2015.7401639.
[34] Kong N, Ha DS, Erturk A, Inman DJ. Resistive impedance matching circuit for piezoelectric energy harvesting. J Intell Mater Syst Struct 2010:1293–302. https://doi.org/10.1177/1045389X09357971.